HHS Public Access

Author manuscript

J Magn Reson Imaging. Author manuscript; available in PMC 2019 May 01.

Published in final edited form as:

J Magn Reson Imaging. 2018 May ; 47(5): 1260–1267. doi:10.1002/jmri.25867.

In vivo assessment of the placental anatomy and perfusion in a mouse model of intrauterine inflammation

Dan Wu, PhD[1,*], **Jun Lei, PhD**[2], **Bei Jia, MD**[2,3], **Han Xie, MD**[2,4], **Yan Zhu, MD**[2,5], **Jiadi Xu, PhD**[1,6], **Susumu Mori, PhD**[1,6], **Jiangyang Zhang, PhD**[7], and **Irina Burd, MD, PhD**[2]

[1]The Russell H. Morgan Department of Radiology and Radiological Science, The Johns Hopkins University School of Medicine, Baltimore, MD, USA

[2]Department of Gynecology and Obstetrics, Division of Maternal Fetal Medicine, The Johns Hopkins University School of Medicine, Baltimore, MD, USA

[3]Department of Gynecology and Obstetrics, Shanghai First Maternity and Infant Hospital, Tongji University School of Medicine, Shanghai, China

[4]Center for Prenatal and Hereditary Disease Diagnosis, Department of Obstetrics and Gynecology, Nanfang Hospital, Southern Medical University, Guangzhou, China

[5]Department of Gynecology and Obstetrics, Xinqiao Hospital, Third Military Medical University, Chongqing, China

[6]F.M. Kirby Research Center for Functional Brain Imaging, Kennedy Krieger Institute, Baltimore, MD, USA

[7]Bernard and Irene Schwartz Center for Biomedical Imaging, Department of Radiology, New York University School of Medicine, New York, NY, USA

Abstract

Background—MRI provides useful markers to examine placental function. MRI features of placental injury due to intrauterine inflammation—a common risk during pregnancy, are not well-known.

Purpose—We aim to investigate the capability of structural MRI and intra-voxel incoherent motion (IVIM) imaging in examining acute placental injury in a mouse model of intrauterine inflammation, as well as gestation-dependent placental changes.

Study Type—Prospective study.

Animal Model—Pregnant CD1 mice were scanned on embryonic day 15 (E15, n=40 placentas from six dams) and E17. On E17, mice were subjected to intrauterine injury by exposure to lipopolysaccharide (LPS, n=25 placentas from three dams) or sham injury (n=25 placentas from three dams).

Correspondence to: Dan Wu, Ph.D., Department of Radiology, Johns Hopkins University School of Medicine, Traylor 210, 720 Rutland Ave., Baltimore, MD, 21205, dwu18@jhu.edu, Phone: (410) 516-3826.

Field Strength/Sequence—*In vivo* MRI was performed on an 11.7 Tesla Bruker scanner, using a fast spin-echo sequence and a diffusion-weighted echo-planar imaging (EPI) sequence.

Assessment—T2-weighted MRI was acquired to evaluate placental volume. IVIM imaging was performed in a restricted field-of-view using 15 b-values from 10–800 s/mm^2, based on which, the pseudo-diffusion fraction (f), pseudo-diffusion coefficient (D^*), and tissue water coefficient (D) were estimated with a two-step fitting procedure.

Statistical Tests—Two-way ANOVA was used to evaluate the group differences.

Results—The placental volume increased by approximately 21% from E15 to E17 ($p<0.01$), and a 15% volume loss was observed at 6hrs after LPS exposure ($p<0.01$). IVIM parameters (f, D^*, and $f{\cdot}D^*$) were similar between the E15 and E17 sham groups ($p>0.05$), which significantly reduced in the LPS-exposed placentas compared to the shams ($p<0.001$). D values decreased from E15 to E17 ($p<0.05$), which were further reduced after LPS exposure ($p<0.05$). Decreased placental area and vascular density were histologically identified in the LPS-exposed group, along with gestation-dependent changes.

Data Conclusion—Our results suggested structural MRI and IVIM measurements are potential markers for detecting acute placental injury after intrauterine inflammation.

Keywords

Intravoxel-incoherent motion; placental perfusion; placental volume; intrauterine inflammation; gestation

INTRODUCTION

The placenta plays a central role in determining pregnancy outcomes, and maternal and fetal health (1–3). Placental dysfunction is known to be associated with adverse pregnancy outcomes, such as stillbirth, fetal growth restriction, preterm birth, and preeclampsia (4,5). MRI is a safe and useful supplemental diagnostic tool in pregnancy (6). The development of MRI tools has been an important component of the human placenta project (7) to noninvasively probe the placental functions. A range of MRI techniques have been proposed to examine the placenta, including anatomical measures using T1- and T2-weighted (8), and diffusion-weighted MRI (9); and functional measures using dynamic contrast enhanced MRI (DCE) (10), arterial spin labelling (ASL) (11), intravoxel incoherent motion (IVIM) imaging (12), and blood oxygen level-dependent (BOLD) MRI (13). Excellent reviews can be found in (14,15). Particularly, the IVIM technique (16) provides unique information about blood flow in the capillary and small vessels, without exogenous administration of contrast-agent as required for DCE. IVIM measures of the placental perfusion have been reported in human with normal or complicated pregnancy (8,17–20), and animal models with normal pregnancy (12,21). The IVIM-derived indices, such as the pseudo-diffusion fraction (f) and its product with the pseudo-diffusion diffusivity (D^*), have been related to blood volume and blood flow velocity in the capillary bed (22). The technique can be a promising tool to investigate maternal vascular malperfusion of placenta.

Intrauterine inflammation is the one of the most common scenario associated with perinatal complications (23). Infection-induced maternal immune activation leads to a chain of inflammatory response mediated by cytokines (24), resulting in placental injury, fetal brain injury, and adverse fetal outcomes. However, radiological features of placental injury that results from intrauterine inflammation, are not well known. In this study, we utilize a mouse model of intrauterine inflammation (25,26) that replicates this clinical scenario. This model employs an endotoxin, lipopolysaccharide (LPS, a component of the cell wall of gram negative bacteria), which induces maternal cytokine production from the maternal serum, uterus, placenta, and in the fetal brain, similar to the cytokine signaling pathway in human. The model exhibits a well-defined phenotype of fetal brain injury, including white matter damage and neuro-inflammation (27,28), as well as pathological evidences of placental injury (29). We hypothesized that acute changes in placenta anatomy and perfusion after intrauterine inflammation are detectable by *in vivo* MRI. Our pre-clinical study aims to provide a solid translational backdrop for clinically useful and safe placental assessments in settings of inflammation-related pregnancy disorders.

Common challenges in placenta MRI include motion artifacts resulting from the fetal movement and maternal respiratory motion, as well as field inhomogeneity due to the tissue, blood, air, and fat around the placenta in the abdomen space. Furthermore, the mouse uterine environment is known to be very hypoxic compared to humans (30). The mouse placenta has high content of deoxygenated blood, which has very short T2 and T2* relaxation time at high field (31,32), and thereby results in low signal-to-noise ratio (SNR). In this study, we performed IVIM using single-shot echo planar imaging (EPI), with a restricted field-of-view (FOV) and a high-sensitivity imaging coil, to potentially mitigate the above-mentioned issues. We investigated the capability of anatomical and IVIM-based capillary perfusion measurements in detecting 1) gestation-dependent changes in the mouse placenta at two gestational stages; and 2) acute placental injury in the mouse model of intrauterine inflammation.

MATERIALS AND METHODS

Animal Preparation

All experimental procedures were approved by the Animal Use and Care Committee at the study site. Pregnant CD-1 mice (Charles River Laboratories, Wilmington, MA) with an average litter size of 11 pups and full term gestation of 19 days were used for this study. Six pregnant dams were scanned on embryonic day 15 (E15). On E17, three of the six dams were subjected to intrauterine inflammation, as previously described in (26–28). Briefly, pregnant dams were placed under isoflurane anesthesia and a mini laparotomy was performed. Lipopolysaccharide (LPS, Sigma, St. Louis, MO, Lot. 102M4017V) of 25 μg in a 100 μL phosphate-buffered solution (PBS) was injected between two gestational sacs in the lower uterine horn. The other three dams underwent the same procedure but were injected with 100 μL PBS as sham controls. Routine laparotomy closure was performed and the dams recovered.

In vivo MRI

Naïve pregnant mice were scanned on E15 (n=6), and they were imaged again on E17 at 6 hrs after LPS-exposure (n=3) or sham surgery (n=3). During imaging, mice were anesthetized with isoflurane (1%), together with air and oxygen mixed at a 3:1 ratio, via a vaporizer. Respiration was monitored via a pressure sensor (SAII, Stony Brook, NY).

In vivo MRI was performed on an 11.7 Tesla horizontal Bruker scanner (Bruker Biospin, Billerica, MA, USA) with a 72-mm diameter quadrature volume transmitter coil. Images were acquired with a 15mm planar surface receive-only coil, which was attached to one side of the mouse abdomen using soft cloth surgical tapes, and the coil commonly covered about five placentas in one of the uterus horns. This provided a restricted field-of-view (FOV) and relatively high signal-to-noise ratio (SNR). Saturation slices were placed in the phase-encoding direction around the FOV to avoid residual signal fold-over. After completing imaging in one of the uterus horns, we re-positioned the coil to the other side to image additional placentas. The experimental setup is illustrated in Figure 1D.

T2-weighted anatomical images were acquired using a fast spin-echo sequence at a FOV of 28.8 mm × 24 mm, in-plane resolution of 0.15 × 0.15 mm^2, 20 slices with 1 mm thickness, echo time (TE)/ repetition time (TR) = 24/3000ms, eight spin echoes, and scan time of 6 minutes with respiration triggers. IVIM imaging was performed with a diffusion-weighted single-shot echo-planar imaging (EPI) sequence at the same FOV, in-plane resolution of 0.3 × 0.3 mm^2, 20 slices with 1 mm thickness, two signal averages, TE/TR = 32/5000ms, 15 b-values ranging from 0 to 800 s/mm^2 (b = 0, 10, 25, 50, 75, 100, 125, 150, 200, 300, 400, 500, 600, 700, and 800 s/mm^2), six directions, two repetitions, and scan time of 30 minutes with respiration triggers.

Image Analysis

The placental regions-of-interest (ROIs) were manually delineated based on the T2-weighted images (Figure 1C) using ROIEditor (www.mristudio.org) for volumetric analysis. Only the placentas with a SNR (ratio between the mean signals in the placental ROI versus the standard deviation of the background signals) above 20 in the non-diffusion-weighted (b_0) image was used in IVIM analysis. The IVIM data were first averaged over six diffusion directions to obtain mean diffusion-weighted images at each b-value, and then the IVIM fitting was performed following a two-step procedure in Matlab (www.mathworks.com), as described in (12). Briefly, in the first step, parameters were estimated with approximations. The water diffusivity D was approximated with a mono-exponential fitting of the high b-value (b > 300 s/mm^2) data, according to a mono-exponential decay $S/S_1 = e^{-b \cdot D}$, and S_1 was simultaneously obtained from the fitting as the approximated tissue water signal. The pseudo-diffusivity D^* was approximated at 10 times of D. The total non-diffusion-weighted signal (S_0) was approximated by extrapolating the low b-value (b = 10–100 s/mm^2) data, and then the pseudo-diffusion fraction f was approximated as $(S_0 - S_1)/S_0$. In the second step, a bi-exponential fitting $S/S_0 = f \cdot e^{-b \cdot D^*} + (1-f) \cdot e^{-b \cdot D}$ was performed at each voxel, using boundary constraints based on the approximated f, D, and D^* values from the first step, e.g., fitting of f and D was constrained within 50% –150% of the approximated values, and D^* was constrained within 30% – 300% of the approximated value.

Immunohistochemistry

Pregnant dams were euthanized with carbon dioxide, and five placentas were dissected from each group (E15, E17 PBS and LPS groups). The isolated placentas were fixed overnight at 4°C in 4% paraformaldehyde. Samples were cut using a cryostat (Leica; Buffalo Grove, IL) at 20 μm thickness and mounted on positively charged slides (Fischer Scientific), followed by drying at room temperature. Tissues were then incubated with rabbit anti-vimentin antibody (endothelia marker, 1:200, Abcam, Cambridge, MA) overnight at 4°C, along with DAPI for counter staining, and images were viewed using a Zeiss Axioplan 2 Microscope System. Density of the Vimentin expression was calculated by Vimentin positive area divided by the total area in a local patch in labyrinth of placenta, using Image J at 20× magnification. Five patches were randomly captured in the labyrinth, and densities were averaged among the patches for each placenta. The middle level of each placenta were used to evaluate the placenta size by measuring the cross-sectional area. The outlines of each placental sample were manually delineated based on DAPI counter stained sections, using a Freehand Line tool in Image J, and the cross-sectional areas were automatically calculated based on the measurement scale. The procedure was repeated five times for each sample and the average number was used.

Statistical Analysis

The placental volumes and IVIM-derived parameters were obtained for the E15 naïve, E17 PBS, and E17 LPS groups. Voxelwise f, D^*, D, and $f{\cdot}D^*$ values were averaged over each placenta for group analysis. Pairwise group differences were analyzed using two-way ANOVA in Graphpad (graphpad.com/scientific-software/prism/). Since multiple placentas were obtained from the same dam, the dam difference was considered as one factor, in addition to the gestational age or intrauterine injury effects.

RESULTS

Placenta volumes were obtained based on T2-weighted images in 43 placentas from six E15 dams, 30 placentas from three E17 sham dams, and 30 placentas from three E17 dams at 6hrs after exposure to LPS (Figure 1 A–C). ROI analysis showed significant increase of placenta volume from E15 (93.6 ± 15.0 mm^3) to E17 (PBS group, 120.5 ± 25.3 mm^3, $p<0.001$), and a significant reduction in the LPS group (100.0 ± 15.3 mm^3, $p<0.001$) compared to the PBS group (Figure 1E). This matched well with histologic measures of placenta cross-sectional areas (Fig. 4C), which showed about 18% increase from E15 to E17 and 16% reduction after LPS exposure.

IVIM analysis was performed in 40 placentas from the E15 dams, 25 placentas from E17 sham dams, and 25 placentas from E17 LPS dams. The SNR of the b_0 images were 38.4 ± 13.4, 32.1 ± 13.5, and 30.6 ± 12.3 in the E15, E17 PBS, and LPS groups, respectively. Examples of the diffusion signal attenuation patterns and IVIM fitting results were shown in Figure 3. The signal intensities followed a bi-exponential attenuation at b-values of 0–800 s/mm^2, in each individual diffusion directions in a normal E17 placenta (Figure 2A). Figure 2B showed the averaged diffusion signals in an E15, an E17 PBS, and a LPS placenta, along with the IVIM fitting curves. Corresponding voxel-wise fitting results of f and D^* were

mapped on the $b_0$images in Figure 3C. Reduced intensity in the *f* and *D** maps of the LPS-exposed placenta were observed, which corresponded to the smaller signal attenuation in its attenuation curves. Statistical analysis revealed significantly lower *f* values in the E17 LPS group (0.22±0.02) compared to the E17 PBS groups (0.25±0.02, p<0.01), controlled by the dam differences (Figure 3A). LPS exposure also led to lower *D** values ($6.22\pm1.31\times10^{-3}$ mm^2/s) compared to PBS group ($8.67\pm1.87\times10^{-3}$ mm^2/s, p<0.001). The composite measure of *f*·*D** was much lower in the E17 LPS-exposed placentas ($1.33\pm0.30\times10^{-3}$ mm^2/s) than that in the E17 PBS group ($2.15\pm0.56\times10^{-3}$ mm^2/s, p <0.001). We did not observe gestation dependent changes in either *f*, *D**, or *f*·*D** between E15 and E17 PBS placentas. The tissue diffusivity *D* values decreased from E15 ($0.81\pm0.16\times10^{-3}$ mm^2/s) to E17 ($0.71\pm0.15\times10^{-3}$ mm^2/s, p=0.016), which also showed reduction after injury ($0.63\pm0.11\times10^{-3}$ mm^2/s, *p*=0.02 compared to sham) (Figure 3D). Vimentin staining of the micro-vessels in placentas demonstrated an increase of vascular density from E15 to E17 (n=5 placentas per group, p=0.02), and a significant reduction of vascular density after LPS exposure (n=5, p<0.001), which was evident from the stained sections and also quantitative analysis (Fig. 4A–B).

DISCUSSION

In this study, we performed *in vivo* MRI assessments of the gestation-dependent placental volume and capillary blood perfusion, and their changes in response to acute intrauterine inflammatory injury in a mouse model. It is known that the placenta grows substantially with gestational age (33), and the volumetric measure has been shown to be a useful indicator of placental integrity and pregnancy outcome, e.g., placental volume was correlated with birth weight (34) and lower volume was associated with adverse fetal outcome, such as small for gestational age (35). Our results showed increased placental volume (~ 21%) in the normal pregnant dams from E15 to E17. The reduction of placental volume (~ 15%) observed at 6hrs after LPS exposure indicated acute placental tissue injury in this model. Note that compartmentalized analysis of the fetal and maternal parts was not performed in this study due to the lack of contrast to accurately define the fetal and maternal boundary.

The IVIM technique accesses blood microcirculation in the capillary network (16,22,36,37), and separate it from tissue water diffusion by a bi-exponential fitting; whereas the fast blood flow in the large vessels is mostly spoiled by the diffusion gradients. Therefore, the IVIM indices provide important information about the capillary perfusion in addition to standard perfusion MRI (10,11), and has been extensively used in the brain and several body organs (37). The placenta is a highly vascular organ, in which the blood takes up about 50% of the whole placenta volume (8). Our measurement of capillary blood fraction (*f*) of approximately 25% with respect to the tissue water, as well as the *D* and *D** values agreed with previous studies in the mouse placenta under normal conditions (21). Gestation-dependent changes in IVIM measurements in normal pregnancy has been investigated earlier. For example, Sohlberg et al. (20) reported a decrease in *f* from early (<34 weeks) to late (≥34 weeks) gestation; Moore et al. (17) showed largely unchanged *f* during gestation (20–42 weeks). Our results showed no apparent changes in the IVIM indices (*f*, *D**, and *f*·*D**) from E15 to E17. Yet, the Vimentin expression indicated an increase of vascular density from E15 to E17. This observation suggested that IVIM may not be sensitive to detect small perfusional changes with gestation; but note that the IVIM measurements

mainly reflect microcirculation in the capillary bed, which do not necessary perfectly match with the Vimentin staining that labels endothelium cells of vessels. These factors needs to be taken into consideration when interpreting both human and animal studies.

Although the IVIM measurements may not be sufficient to capture the gestational changes between E15 and E17, all IVIM indices showed acute reductions at 6hrs after intrauterine inflammation (Fig. 3). Particular, we observed signification decrease in f, which relates to capillary blood volume, in the LPS-exposed placentas compared to the PBS controls; and even more so in $f{\cdot}D^*$, which relates to capillary blood flow velocity. These changes pointed to injury to the vasculature and a disruption in blood flow, which may collectively contribute to the development of thrombosis (clot formation) and placental volume loss. The results were supported by the damage of placental vasculature seen in the pathology, e.g., Vimentin staining revealed extensive reduction of vascular density in the LPS group compared to the PBS group (Fig. 4A–B). Therefore, the IVIM technique offered sensitive markers to acute placental malperfusion after intrauterine inflammation.

IVIM is well suited for imaging the placenta as it contains large pools of atrial and venous blood. However, the short T2 and T2* relaxation of highly hypoxic deoxygenated blood in the mouse placenta make it challenging to perform IVIM on high field MRI systems. For example, venous blood T2 is estimated to be around 14 ms at 11.7T (31), and venous blood T2* can be as short as 4 ms at 7T (32). To compensate the signal loss, we used a high sensitivity planar surface coil that was attached to the lower abdomen to restrict the FOV and increase SNR (approximately three times higher SNR than a mouse body coil). With the small FOV, the readout time and echo time of a single-shot EPI can be reduced to compensate for the short T2 and T2*. In addition, we excluded the low SNR placenta data in the analysis, and we took a two-step fitting procedure with approximated boundary conditions to reduce potential fitting errors. This approach can be further combined with the localized imaging technique with spatially selective excitation pulse that we used for fetal brain MRI (38) to obtain 3D high-resolution MRI of individual placentas, which may enable 3D shape analysis and texture analysis in addition to the volumetric measure.

There are several limitations in the current study. Firstly, it is difficult to accurately track individual placentas in a longitudinal study, e.g., from E15 to E17 in this study. The embryos and placentas are not necessarily positioned according to their order along the uterine horn in the crowded 3D uterine space. Their relative positions depend on the available free space in the maternal abdomen and the positions can change from day to day in longitudinal studies. Advanced techniques (39) utilizing the specific pattern of dual arterial blood supply in the mouse uterine may help to resolve this complexity. Secondly, although we shortened the echo time (~30ms) with the small FOV approach, blood signals had faster T2/T2* decay than tissue water signals, and thereby, the perfusion component could be underestimated in the IVIM model. The use of both flow-compensated and non-compensated gradients (40) may potentially untangle the interaction between relaxation and diffusion effects. In addition, we realize that although the use of planar surface coil helped to improve the SNR, but it was only beneficial to the placentas located near the surface of the abdomen, which limited the throughput of the imaging. Hardware development of customized coils would greatly advance preclinical *in utero* studies.

In conclusion, our results demonstrated that volumetric and IVIM measurements were able to capture acute changes in placental anatomy and perfusion in response to intrauterine inflammation. These *in vivo* techniques potentially provide clinically useful assessments to the spectrum of placental dysfunction associated with vascular malperfusion, with early diagnosis targeted for prevention of further deterioration.

Acknowledgments

Grant supports: This work is made possible by the following research funding: R21 NS098018, K08 HD073315, and R01 HD074593.

References

1. Ananth CV, Friedman AM. Ischemic placental disease and risks of perinatal mortality and morbidity and neurodevelopmental outcomes. Seminars in Perinatology. 2014; 38(3):151–158. [PubMed: 24836827]
2. Longtine MS, Nelson DM. Placental Dysfunction and Fetal Programming: The Importance of Placental Size, Shape, Histopathology, and Molecular Composition. Seminars in Reproductive Medicine. 2011; 29(3):187–196. [PubMed: 21710395]
3. Ptacek I, Sebire NJ, Man JA, Brownbill P, Heazell AEP. Systematic review of placental pathology reported in association with stillbirth. Placenta. 2014; 35(8):552–562. [PubMed: 24953162]
4. Apel-Sarid L, Levy A, Holcberg G, Sheiner E. Term and preterm (<34 and <37 weeks gestation) placental pathologies associated with fetal growth restriction. Arch Gynecol Obstet. 2010; 282(5): 487–492. [PubMed: 19855989]
5. Silasi M, Cohen B, Karumanchi SA, Rana S. Abnormal placentation, angiogenic factors, and the pathogenesis of preeclampsia. Obstet Gynecol Clin North Am. 2010; 37(2):239–253. [PubMed: 20685551]
6. Levine D. Obstetric MRI. J Magn Reson Imaging. 2006; 24(1):1–15. [PubMed: 16736491]
7. Guttmacher AE, Maddox YT, Spong CY. The Human Placenta Project: Placental structure, development, and function in real time. Placenta. 2014; 35(5):303–304. [PubMed: 24661567]
8. Gowland P. Placental MRI. Semin Fetal Neonatal Med. 2005; 10(5):485–490. [PubMed: 16027055]
9. Sivrioglu AK, Ozcan UA, Turk A, et al. Evaluation of the placenta with relative apparent diffusion coefficient and T2 signal intensity analysis. Diagnostic and Interventional Radiology. 2013; 19(6): 495–500. [PubMed: 24047717]
10. Frias AE, Schabel MC, Roberts VH, et al. Using dynamic contrast-enhanced MRI to quantitatively characterize maternal vascular organization in the primate placenta. Magn Reson Med. 2015; 73(4):1570–1578. [PubMed: 24753177]
11. Derwig I, Lythgoe DJ, Barker GJ, et al. Association of placental perfusion, as assessed by magnetic resonance imaging and uterine artery Doppler ultrasound, and its relationship to pregnancy outcome. Placenta. 2013; 34(10):885–891. [PubMed: 23937958]
12. Solomon E, Avni R, Hadas R, et al. Major mouse placental compartments revealed by diffusion-weighted MRI, contrast-enhanced MRI, and fluorescence imaging. Proceedings of the National Academy of Sciences of the United States of America. 2014; 111(28):10353–10358. [PubMed: 24969421]
13. Sorensen A, Peters D, Simonsen C, et al. Changes in human fetal oxygenation during maternal hyperoxia as estimated by BOLD MRI. Prenatal Diagnosis. 2013; 33(2):141–145. [PubMed: 23233459]
14. Andescavage NN, du Plessis A, Limperopoulos C. Advanced MR imaging of the placenta: Exploring the in utero placenta-brain connection. Semin Perinatol. 2015; 39(2):113–123. [PubMed: 25765905]
15. Avni R, Neeman M, Garbow JR. Functional MRI of the placenta – From rodents to humans. Placenta. 36(6):615–622.

16. Lebihan D, Breton E, Lallemand D, Grenier P, Cabanis E, Lavaljeantet M. Mr Imaging of Intravoxel Incoherent Motions - Application to Diffusion and Perfusion in Neurologic Disorders. Radiology. 1986; 161(2):401–407. [PubMed: 3763909]
17. Moore RJ, Issa B, Tokarczuk P, et al. In vivo intravoxel incoherent motion measurements in the human placenta using echo-planar imaging at 0.5 T. Magnet Reson Med. 2000; 43(2):295–302.
18. Moore RJ, Ong SS, Tyler DJ, et al. Spiral artery blood volume in normal pregnancies and those compromised by pre-eclampsia. Nmr in Biomedicine. 2008; 21(4):376–380. [PubMed: 17893947]
19. Moore RJ, Strachan BK, Tyler DJ, et al. In utero perfusing fraction maps in normal and growth restricted pregnancy measured using IVIM echo-planar MRI. Placenta. 2000; 21(7):726–732. [PubMed: 10985977]
20. Sohlberg S, Mulic-Lutvica A, Lindgren P, Ortiz-Nieto F, Wikström AK, Wikström J. Placental perfusion in normal pregnancy and early and late preeclampsia: A magnetic resonance imaging study. Placenta. 2014; 35(3):202–206. [PubMed: 24529946]
21. Alison M, Chalouhi GE, Autret G, et al. Use of Intravoxel Incoherent Motion MR Imaging to Assess Placental Perfusion in a Murine Model of Placental Insufficiency. Investigative Radiology. 2013; 48(1):17–23. [PubMed: 23192161]
22. Federau C, O'Brien K, Meuli R, Hagmann P, Maeder P. Measuring brain perfusion with intravoxel incoherent motion (IVIM): Initial clinical experience. Journal of Magnetic Resonance Imaging. 2014; 39(3):624–632. [PubMed: 24068649]
23. Goldenberg RL, Hauth JC, Andrews WW. Intrauterine infection and preterm delivery. The New England journal of medicine. 2000; 342(20):1500–1507. [PubMed: 10816189]
24. Hsiao EY, Patterson PH. Activation of the maternal immune system induces endocrine changes in the placenta via IL-6. Brain, behavior, and immunity. 2011; 25(4):604–615.
25. Burd I, Balakrishnan B, Kannan S. Models of fetal brain injury, intrauterine inflammation, and preterm birth. Am J Reprod Immunol. 2012; 67(4):287–294. [PubMed: 22380481]
26. Burd I, Bentz AI, Chai J, et al. Inflammation-induced preterm birth alters neuronal morphology in the mouse fetal brain. Journal of neuroscience research. 2010; 88(9):1872–1881. [PubMed: 20155801]
27. Burd I, Chai J, Gonzalez J, et al. Beyond white matter damage: fetal neuronal injury in a mouse model of preterm birth. Am J Obstet Gynecol. 2009; 201(3):279, e271–278. [PubMed: 19733279]
28. Burd I, Bentz A, Gonzalez J, et al. Inflammation-induced preterm birth alters neuronal morphology in the mouse fetal brain. Journal of Neuroscience Research. 2010 In press.
29. Eloundou SN, Wu D, Alshehri W, Zhang J, Burd I. Acute MRI changes in mouse placentas exposed to intrauterine inflammation. Am J Obstet Gynecol. 2016; 214(1):S311–S312.
30. Lee YM, Jeong CH, Koo SY, et al. Determination of hypoxic region by hypoxia marker in developing mouse embryos in vivo: a possible signal for vessel development. Dev Dyn. 2001; 220(2):175–186. [PubMed: 11169851]
31. Grgac K, Li W, Huang A, Qin Q, van Zijl PCM. Transverse water relaxation in whole blood and erythrocytes at 3T, 7T, 9.4T, 11.7T and 16.4T; determination of intracellular hemoglobin and extracellular albumin relaxivities. Magnetic Resonance Imaging. 2017; 38:234–249. [PubMed: 27993533]
32. Ogawa S, Lee TM, Nayak AS, Glynn P. Oxygenation-Sensitive Contrast in Magnetic-Resonance Image of Rodent Brain at High Magnetic-Fields. Magnet Reson Med. 1990; 14(1):68–78.
33. Andescavage, NN., Yarish, A., Serag, A., et al. Pediatric Academic Societies and Asian Soceity for Pediatric Research. Vancouver, Canada: 2014. Quantitative 3D MRI Assessment of Placental Volume in Healthy and Complex Pregnancies.
34. Derwig IE, Akolekar R, Zelaya FO, Gowland PA, Barker GJ, Nicolaides KH. Association of placental volume measured by MRI and birth weight percentile. J Magn Reson Imaging. 2011; 34(5):1125–1130. [PubMed: 21928386]
35. Hafner E, Philipp T, Schuchter K, Dillinger-Paller B, Philipp K, Bauer P. Second-trimester measurements of placental volume by three-dimensional ultrasound to predict small-for-gestational-age infants. Ultrasound in Obstetrics & Gynecology. 1998; 12(2):97–102. [PubMed: 9744052]

36. Lebihan D, Turner R. The Capillary Network - a Link between Ivim and Classical Perfusion. Magnet Reson Med. 1992; 27(1):171–178.

37. Koh DM, Collins DJ, Orton MR. Intravoxel incoherent motion in body diffusion-weighted MRI: reality and challenges. AJR American journal of roentgenology. 2011; 196(6):1351–1361. [PubMed: 21606299]

38. Wu D, Lei J, Rosenzweig JM, Burd I, Zhang JY. In utero localized diffusion MRI of the embryonic mouse brain microstructure and injury. Journal of Magnetic Resonance Imaging. 2015; 42(3):717–728. [PubMed: 25537944]

39. Avni R, Raz T, Biton IE, Kalchenko V, Garbow JR, Neeman M. Unique in utero identification of fetuses in multi-fetal mouse pregnancies by placental bi-directional arterial spin labeling (BD-ASL) MRI. Magnetic resonance in medicine : official journal of the Society of Magnetic Resonance in Medicine / Society of Magnetic Resonance in Medicine. 2012; 68(2):560–570.

40. Ahlgren A, Knutsson L, Wirestam R, et al. Quantification of microcirculatory parameters by joint analysis of flow-compensated and non-flow-compensated intravoxel incoherent motion (IVIM) data. NMR Biomed. 2016; 29(5):640–649. [PubMed: 26952166]

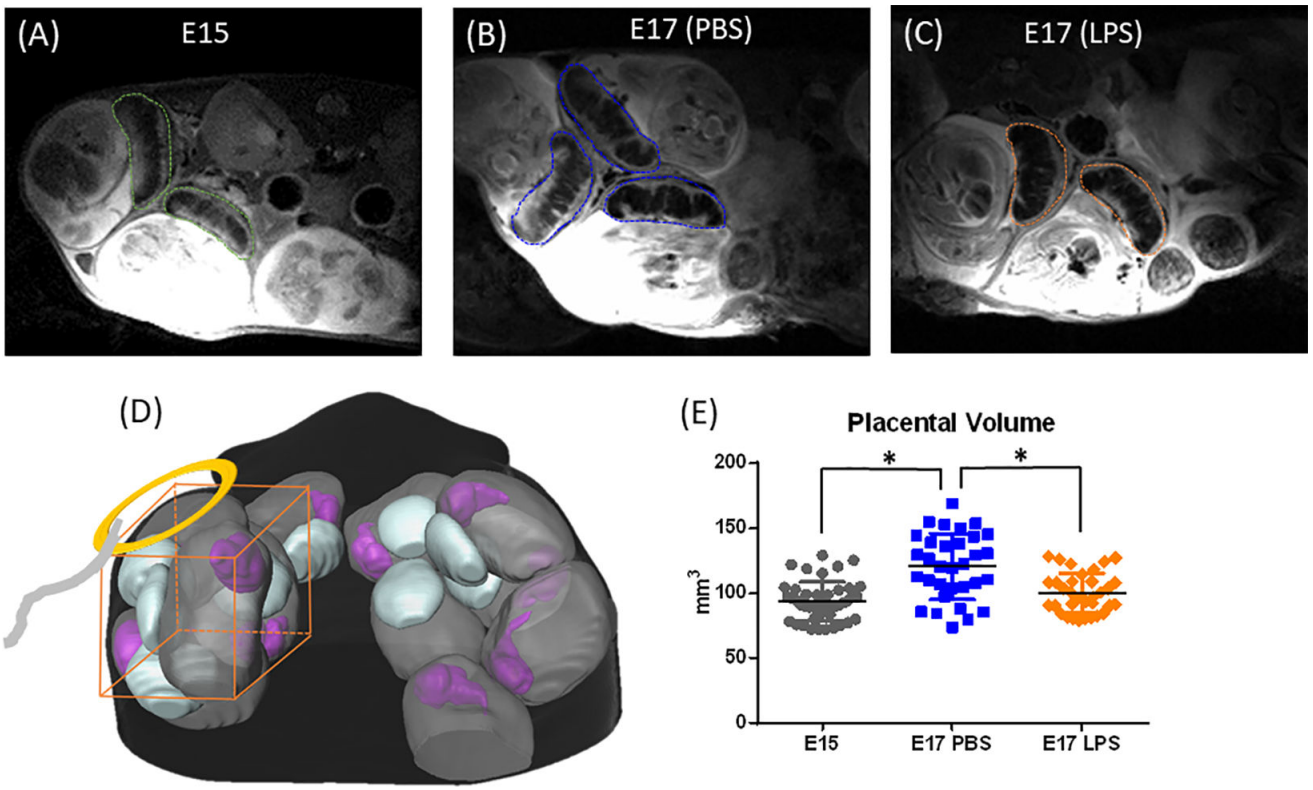

Fig. 1.

Volumetric analysis of the mouse placenta. (A–C) T2-weighted images of the placentas in an E15, an E17 PBS-treated, and an E17 LPS-treated mouse. The dashed contours indicate the manual delineation of the placentas for volumetric analysis. (D) A schematic of the experimental setup with a planer surface coil. (E) A scatter plot of placenta volumes from the E15 (n=43), E17 PBS (n=30) and LPS group (n=30) groups. * $p<0.01$ by one-way ANOVA followed by post-hoc *t*-test with Bonferroni correction.

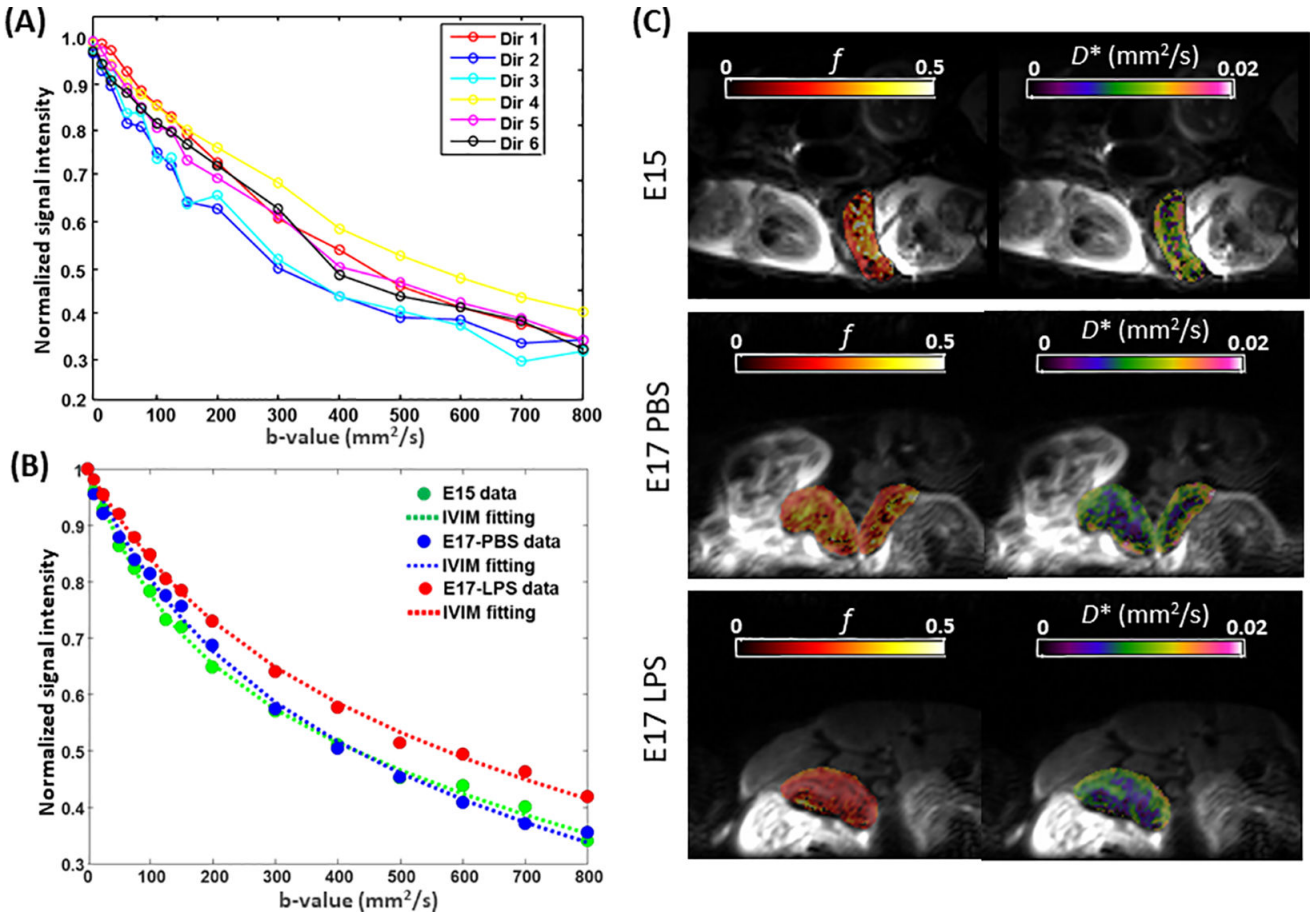

Fig. 2.

IVIM analysis of placental capillary perfusion. (A) Diffusion-weighted signals acquired from a representative E17-PBS placenta at 16 b-values and six diffusion directions. (B) Measured and fitted diffusion-weighted signals in representative E15, E17 PBS, E17 LPS placentas, averaged over six diffusion directions. (C) Maps of the pseudo-diffusion fraction (*f*) and pseudo-diffusion coefficients (*D**) fitted from the IVIM model and mapped onto non-diffusion-weighted images, in an E15, an E17 PBS-treated, and an E17 LPS-treated mouse.

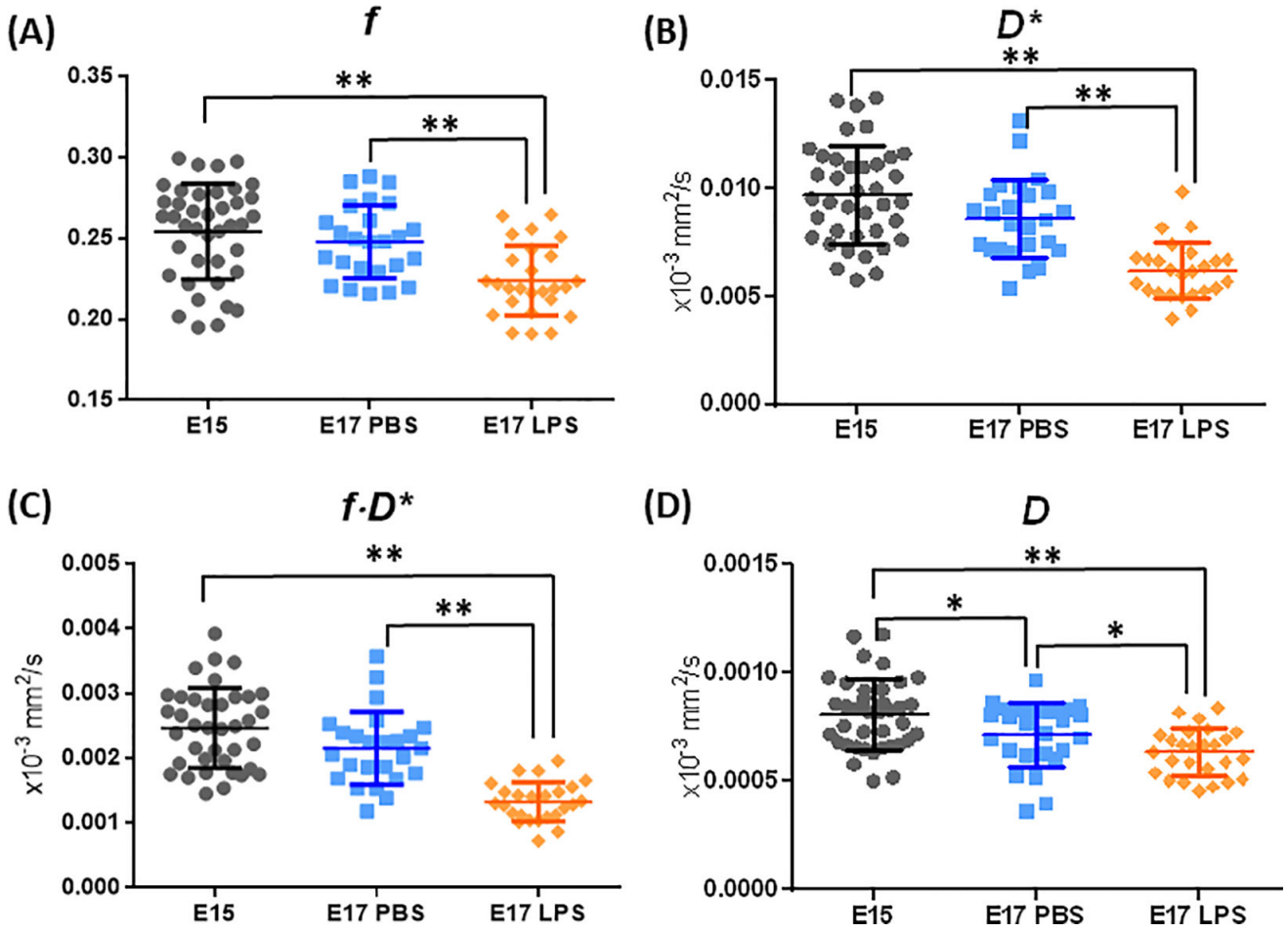

Fig. 3.

Quantitative analysis of the IVIM-based pseudo-diffusion fraction (*f*), pseudo-diffusion confident (*D**), *f*×*D**, and water diffusion coefficient (*D*), in the E15 (n=40), E17 PBS (n=25) and LPS group (n=25) groups. * $p<0.05$ and ** $p<0.001$ indicates group differences by two-way ANOVA, controlled for dam differences.

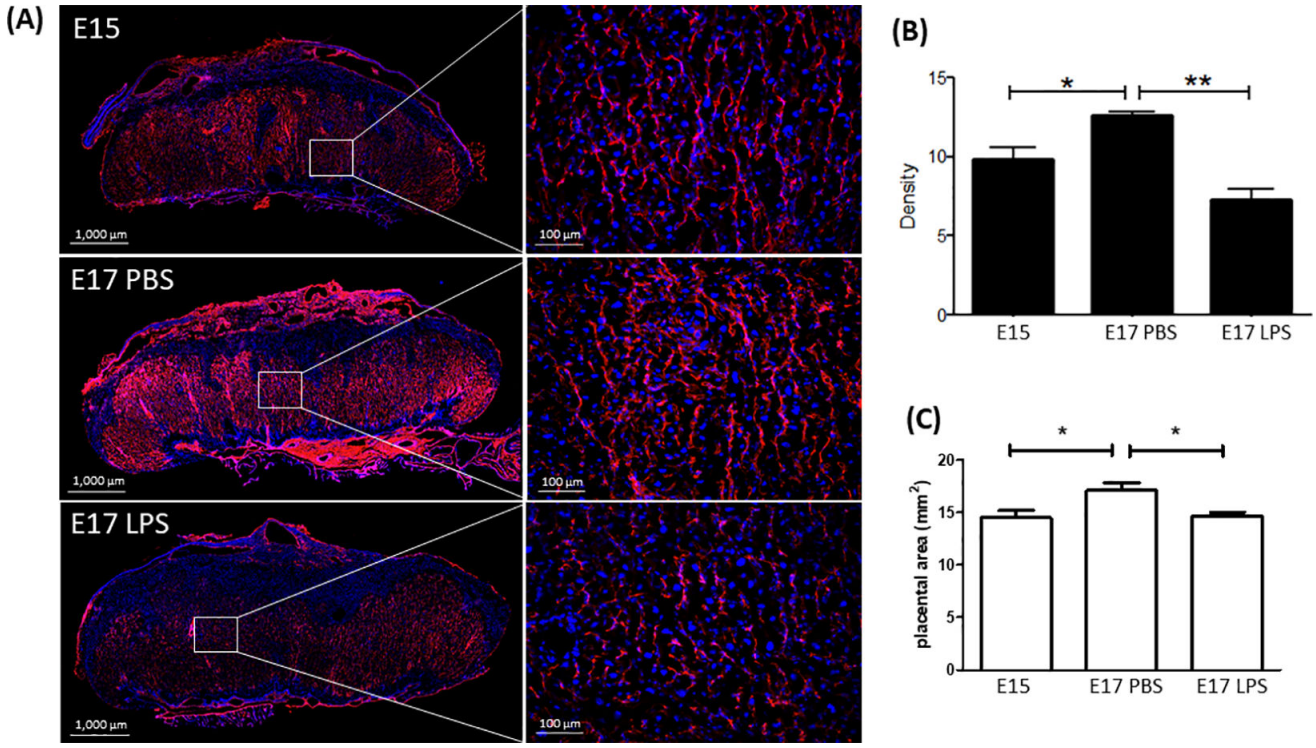

Fig. 4.

Vimentin and DAPI staining of the mouse placentas in E15, E17 PBS, and E17 LPS groups. Representative slices and zoomed-in areas are shown in (A). (B) Density of Vimentin expression in the fetal side of placentas in the three groups (n=5 placentas per group). (C) Cross-sectional areas of the center slice in each placenta (n=5 placentas per group). * $p<0.05$ and ** $p<0.001$ by one-way ANOVA, followed by post-hoc pairwise *t*-test.